2025 IEEE 64th Conference on Decision and Control (CDC)
December 10-12, 2025. Rio de Janeiro, Brazil

Control, Learning, and Optimization Methods for Autonomous Multi-Agent Systems in Transportation

Christos G. Cassandras, Karl H. Johansson, and Andreas A. Malikopoulos

2025 IEEE 64th Conference on Decision and Control (CDC) | 979-8-3315-2627-6/25/$31.00 ©2025 IEEE | DOI: 10.1109/CDC57313.2025.11312853

***Abstract*— Emerging mobility systems are an example of Cyber-Physical Systems (CPSs) in which multiple autonomous agents (vehicles) interact with each other as well as with the infrastructure resources (road side units, traffic lights, etc). Control-theoretic and optimization methods provide a rich framework for managing these complex mixed-traffic socio-economic multi-agent systems. Given the complexity involved and the abundance of data now available, it is essential to integrate learning-based methods not only to design optimal controllers with safety guarantees, but to also gain an understanding of human driving behavior, as well as user preferences for the mobility options that intelligent transportation systems provide. The three objectives of this tutorial paper are: (1) Set the stage for emerging mobility systems consisting of both autonomous and human-driven vehicles in a mixed traffic environment by formulating basic optimal control problems for autonomous vehicles that seek to jointly optimize travel time, energy, and comfort while ensuring that safety constraints are always satisfied. (2) Present methods for solving the formulated problems using a combination of optimization techniques and Control Barrier Functions (CBFs) that provide safety guarantees, as well as state of the art learning-based methods to design effective controllers for mixed traffic transportation systems. (3) Address the societal issues accompanying emerging mobility systems, including new metrics that incorporate accessibility and fairness in a transportation network consisting of both autonomous and human-driven vehicles.**

I. Introduction

Emerging mobility systems are an example of Cyber-Physical Systems (CPSs) in which multiple autonomous agents (vehicles) interact with each other as well as with the infrastructure resources (road side units, traffic lights, etc). What makes these systems particularly exciting is the proliferation of Autonomous Vehicles (AVs) that can operate at different automation levels, from limited driver assistance to full self-driving capabilities. When such AVs are equipped with the ability to communicate with each other (V2V) or with the infrastructure (V2I), they are referred to as Connected Autonomous Vehicles (CAVs) and the resulting network as the "internet of vehicles." Since a portion of vehicles are still human-driven (HDVs), we are faced with a multi-agent system where some agents cooperate with each other (the CAVs) while others (the HDVs) are potentially non-cooperative, giving rise to an interesting game setting where subsets of the CAVs may form cooperative coalitions interacting with non-cooperative HDVs which they may induce to behave in accordance to certain objectives while also ensuring system-wide safe operation. Identifying the proper optimization objectives has thus far mostly focused on the operational efficiency of the transportation network without considering how humans perceive the mobility options and features at their disposal when, for instance, they are asked to comply with specific recommendations on route selection or speed limits. Addressing such societal issues remains largely uncharted territory as we seek to achieve a "socially optimal" mobility system. It is clear that control-theoretic and optimization methods provide a rich framework for managing these complex mixed-traffic socio-economic multi-agent mobility systems. Given the complexity involved and the abundance of data now available, it is essential to integrate learning-based methods not only to design optimal controllers with safety guarantees, but to also gain an understanding of human driving behavior, as well as user preferences for the mobility options that intelligent transportation systems provide.

The paper is organized as follows. In Section II, we set the stage for emerging mobility systems consisting of both autonomous and human-driven vehicles in a mixed traffic environment. This involves the basic optimal control problem formulations for autonomous vehicles that seek to jointly optimize travel time, energy, and comfort while ensuring that safety constraints are always satisfied. In Section III, we discuss methods for solving the formulated problems using a combination of decentralized optimization techniques and Control Barrier Functions (CBFs) that have the property of providing safety guarantees at all times. Section IV extends these methods to mixed traffic settings where CAVs must safely interact with Human Driven Vehicles (HDVs). Section V discusses how CAVs can act as both observers of the state of traffic and as actuators. We highlight the state of the art in learning-based methods to design effective controllers for mixed traffic transportation systems. We also show how simple controllers using the estimated and predicted traffic status can dissipate congestion in a given area. Section VI addresses the societal issues accompanying emerging mobility systems, including new metrics that incorporate accessibility

C.G.C's work was supported in part by NSF under grant CNS-2149511, and by ARPAE under grant DE-AR0001282. K.H.J. was supported by Swedish Research Council Distinguished Professor Grant 2017-01078, Knut and Alice Wallenberg Foundation Wallenberg Scholar Grant, and the Swedish Strategic Research Foundation FUSS SUCCESS Grant. AAM's work was supported in part by NSF under Grants CNS-2401007, CMMI-2348381, IIS-2415478, and in part by MathWorks.

C. G. Cassandras is with the Division of Systems Engineering and Center for Information and Systems Engineering, Boston University, Brookline, MA 02446 (email:cgc@bu.edu).

K. H. Johansson is with the School of Electrical Engineering and Computer Science, KTH Royal Institute of Technology, Sweden. He is also affiliated with Digital Futures. (email:kallej@kth.se).

A. A. Malikopoulos is with the School of Civil & Environmental Engineering, Cornell University, Ithaca, New York, U.S.A. E-mails: amaliko@cornell.edu

and fairness in a transportation network consisting of both autonomous and human-driven vehicles.

II. Optimal Control of Autonomous Vehicles

The most significant effect that the control and coordination of CAVs can have in a transportation system arises at critical conflict areas such as merging points (usually, highway on-ramps), roundabouts and intersections. We refer to any such conflict area as a *Control Zone* (CZ) since it is where the best opportunity for cooperative control and optimization exists to efficiently resolve conflicts while ensuring safe interactions among CAVs. Clearly, *decentralized* control mechanisms are preferable, since all computation is performed on board each vehicle and shared only with a small number of other vehicles that are affected by it. Optimal control problem formulations are used in some of these approaches, while Model Predictive Control (MPC) techniques are employed as an alternative, primarily to account for additional constraints and to compensate for disturbances by re-evaluating optimal actions [1], [2]. An alternative to MPC is provided by the use of CBFs [3] exploiting their property to guarantee safety constraints which, in the case of CAVs, is the most crucial requirement for the acceptance and viability of long-awaited self-driving vehicles.

In this section, we set up the basic decentralized optimal control problem that each CAV faces in a CZ. Technical details are limited to one CZ type which, however, captures the key features of the problem. We first consider the case when all vehicles are CAVs. This provides a baseline showing the best (performance upper bound) one can achieve through full cooperation among vehicles before considering the mixed traffic case.

A. Traffic Merging as on Optimal Control Problem

We consider the problem of coordinating CAVs merging from roads, which are generally curved, with the goal of jointly minimizing their travel time and energy consumption as well as passenger discomfort resulting from centrifugal forces experienced at higher speeds during the merging process. The safety constraints include maintaining a speed-dependent safe distance for collision avoidance at the merging point and everywhere throughout the approaching area. The lateral rollover avoidance constraint is obtained through the Zero Moment Point (ZMP) [4] method that is usually used in balancing legged robots.

The case of CAVs traveling and merging along straight roads was analyzed in [5] as an optimal control problem assuming simple linear dynamics for all CAVs. In this case. explicit analytical solutions can be derived, even when all constraints become active. The price to pay for such a complete analytical solution is the computational cost which can range from under 0.1 sec to several seconds whenever multiple constraints become active, in which case one has to derive optimal controls for all constrained arcs along an optimal trajectory. In the case of curved roads, such analytical solutions become intractable, giving us the opportunity to describe an approach where optimal control and CBFs are combined, referred to as *Optimal Control with CBFs* (OCBF). In particular, we first derive an optimal solution when no constraints become active in the optimal control problem. Then, we employ the OCBF framework to optimally track this solution while also guaranteeing the satisfaction of all constraints.

The merging problem arises when traffic must be joined from two different roads, usually associated with a main lane and a merging lane as shown in Fig. 1. We consider the case where all traffic consists of CAVs randomly arriving at the two curved roads joined at the Merging Point (MP) M where a lateral collision may occur. Each segment from the origin O or O' to the merging point M has a length L for both roads and radii $r_{main} > 0, r_{merg} > 0$ for the main and merging roads, respectively. These two segments over which CAVs may communicate with each other and exchange state information is what we referred to earlier as the CZ. CAVs do not overtake each other in the CZ, as each road consists of a single lane. A multi-lane merging problem has been studied in [6] (without road curvatures), in which case overtaking is included. Thus, the problem here can be extended to one with multiple lanes in each road along similar lines.

A coordinator is associated with the MP whose function is to maintain a First-In-First-Out (FIFO) queue of CAVs based on their arrival time at the CZ and to enable real-time communication with the CAVs that are in the CZ, including the last one leaving the CZ. The FIFO assumption, imposed so that CAVs cross the MP in their order of arrival, is made for simplicity and often to ensure fairness, but can be relaxed through dynamic resequencing schemes (e.g., [7]).

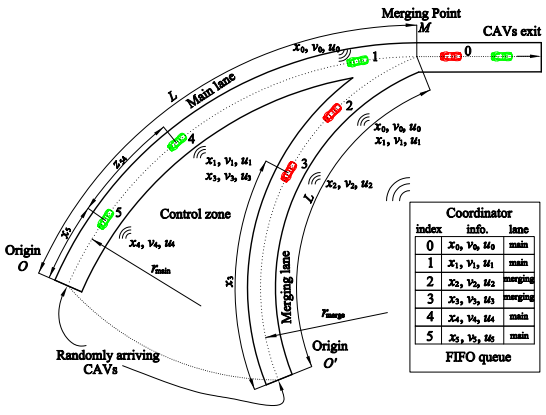

Fig. 1: The merging problem for roads with curvature

Let $F(t)$ be the set of FIFO-ordered (acccording to arrival times at O or O') indices of all CAVs located in the CZ at time t; this includes the CAV (whose index is 0 as shown in Figure 1) that has just left the CZ. Let $N(t)$ be the cardinality of $F(t)$. Thus, if a CAV arrives at O or O' at time t, it is assigned the index $N(t)$. All CAV indices in $F(t)$ decrease by one when a CAV passes over the MP and the vehicle whose index is -1 is dropped.

The vehicle dynamics for each CAV $i \in F(t)$ along the

lane to which it belongs take the form

$$\dot{x}_i(t) = v_i(t), \qquad \dot{v}_i(t) = u_i(t), \tag{1}$$

where $x_i(t)$ denotes the distance to the origin O (O') along the main (merging) lane if the vehicle i is located in the main (merging) lane, $v_i(t)$ denotes the velocity, and $u_i(t)$ denotes the control input (acceleration). We consider three objectives for each CAV subject to four constraints, as detailed next.

Objective 1 (Minimizing travel time): Let t_i^0 and t_i^m denote the time that CAV $i \in F(t)$ arrives at the origin O or O' and the merging point M, respectively. We wish to minimize the travel time $t_i^m - t_i^0$ for CAV i.

Objective 2 (Minimizing energy consumption): We also wish to minimize energy consumption for each $i \in F(t)$:

$$\min_{u_i(t)} \int_{t_i^0}^{t_i^m} C_i(u_i(t))dt, \tag{2}$$

where $C_i(\cdot)$ is a strictly increasing function of its argument, and it usually takes the quadratic form: $C_i(u_i(t)) = u_i^2(t)$. More detailed energy consumption models are possible (e.g., [8]) and are considered in [9].

Objective 3 (Maximizing centrifugal comfort): In order to minimize the centrifugal discomfort (or maximize the comfort), we wish to minimize the centrifugal acceleration

$$\min_{u_i(t)} \int_{t_i^0}^{t_i^m} \kappa(x_i(t))v_i^2(t)dt, \tag{3}$$

where $\kappa : \mathbb{R} \to \mathbb{R}^{\geq 0}$ is the curvature of the road at position x_i. The curvature $\kappa(x_i)$ has a sign which is determined by $\frac{1}{r(x_i)}$, where $r : \mathbb{R} \to \mathbb{R}$ is the radius of the road at x_i. Since we just wish to minimize the centrifugal acceleration, we ignore the sign and set $\kappa(x_i) \geq 0$ in what follows.

Constraint 1 (Safety constraints): Let i_p denote the index of the CAV which physically immediately precedes i in the CZ (if one is present). We require that the distance $z_{i,i_p}(t) := x_{i_p}(t) - x_i(t)$ be constrained by the speed $v_i(t)$ of CAV $i \in F(t)$ so that

$$z_{i,i_p}(t) \geq \varphi v_i(t) + \delta, \quad \forall t \in [t_i^0, t_i^m], \tag{4}$$

where φ denotes the reaction time (as a rule, $\varphi = 1.8$s is used, e.g., [10]). If we define z_{i,i_p} to be the distance from the center of CAV i to the center of CAV i_p, then δ is a constant determined by the length of these two CAVs (taken to be a constant over all CAVs for simplicity).

Constraint 2 (Safe merging): There should be enough safe space at the MP M for a CAV (which eventually becomes CAV 1, as shown in Figure 1) to cut in, i.e.,

$$z_{1,0}(t_1^m) \geq \varphi v_1(t_1^m) + \delta. \tag{5}$$

Constraint 3 (Vehicle limitations): There are constraints on the speed and acceleration for each $i \in F(t)$:

$$\begin{aligned} v_{i,min} \leq v_i(t) \leq v_{i,max}, \quad \forall t \in [t_i^0, t_i^m], \\ u_{min} \leq u_i(t) \leq u_{max}, \quad \forall t \in [t_i^0, t_i^m], \end{aligned} \tag{6}$$

where $v_{i,max} > 0$ and $v_{i,min} \geq 0$ denote the maximum and minimum speed allowed in the CZ, while $u_{min} < 0$ and $u_{max} > 0$ denote the minimum and maximum control, respectively.

Constraint 4 (Lateral safety constraint): Finally, there is a constraint on the centrifugal acceleration to avoid lateral rollover for each $i \in F(t)$:

$$\kappa(x_i(t))v_i^2(t) \leq \frac{w_i^h}{h_i} g, \quad \forall t \in [t_i^0, t_i^m], \tag{7}$$

where $w_i^h > 0$ denotes the half-width of the vehicle, $h_i > 0$ denotes the height of the center of gravity with respect to the ground, and g is the gravity constant. The above lateral safety constraint is obtained through the Zero Moment Point (ZMP) [4] method (assuming the road lateral slope is zero) that balances the CAV considering both gravity and inertia.

Problem Formulation. Our goal is to determine a control law to achieve objectives 1-3 subject to constraints 1-4 for each $i \in F(t)$ governed by the dynamics (1). We first choose $C_i(u_i(t)) = \frac{1}{2}u_i^2(t)$ in (2), noting that the OCBF method allows for more elaborate fuel consumption models, e.g., as in [8]; in what follows, we shall limit ourselves to this model. Normalizing each objective, and combining objectives 1, 2 and 3 with $\alpha_1 \in [0,1], \alpha_2 \in [0, 1-\alpha_1]$, we formulate the following optimal control problem for each CAV:

$$\begin{aligned} \min_{u_i(t), t_i^m} \int_{t_i^0}^{t_i^m} [\alpha_1 + \alpha_2 \frac{\kappa(x_i(t))v_i^2(t)}{\kappa_{\max} v_{\max}^2} \\ + (1-\alpha_1-\alpha_2) \frac{\frac{1}{2}u_i^2(t)}{\frac{1}{2}u_{\lim}^2}]dt, \end{aligned} \tag{8}$$

subject to (1), (4), (27), (6), (7), the initial and terminal position conditions $x_i(t_i^0) = 0$, $x_i(t_i^m) = L$, and given t_i^0, v_i^0 (where v_i^0 denotes the initial speed), and $u_{\lim} := \max\{u_{\max}^2, u_{\min}^2\}$. Observe that the merging time t_i^m is a decision variable in this problem. Finally, the weight factor $\alpha_1 \geq 0, \alpha_2 \geq 0$ can be adjusted to penalize travel time and comfort relative to the energy cost.

Multiplying (8) by $\frac{u_{\lim}^2}{2(1-\alpha_1-\alpha_2)}$ and letting

$$\beta_1 = \frac{\alpha_1 u_{\lim}^2}{2(1-\alpha_1-\alpha_2)}, \quad \beta_2 = \frac{\alpha_2 u_{\lim}^2}{2(1-\alpha_1-\alpha_2)\kappa_{\max} v_{\max}^2} \tag{9}$$

we have a simplified and normalized version of (8):

$$\min_{u_i(t), t_i^m} \int_{t_i^0}^{t_i^m} \left[\beta_1 + \beta_2 \kappa(x_i(t))v_i^2(t) + \frac{1}{2}u_i^2(t)\right] dt. \tag{10}$$

B. Decentralized Online Control

Note that (10) can be locally solved by each CAV i provided that there is some information sharing with only two other CAVs: CAV i_p which physically immediately precedes i and is needed in (4) and CAV $i-1$ so that i can determine whether this CAV is located in the same road or not. With this information, CAV i can determine which of two possible cases applies: (i) $i_p = i-1$, i.e., i_p is the CAV immediately preceding i in the FIFO queue (e.g., $i = 3, i_p = 2$ in Fig. 1), and (ii) $i_p < i-1$, which implies that CAV $i-1$ is in a different road from i (e.g., $i = 4, i_p = 1, i-1 = 3$ in Fig. 1). It is now clear that we can solve problem (10) for any

$i \in F(t)$ in a decentralized way in the sense that CAV i needs only its own local state information and state information from $i-1$, as well as from i_p in case (ii) above. Observe that if $i_p = i-1$, then (27) is a redundant constraint; otherwise, we need to separately consider (4) and (27). Therefore, we will analyze each of these two cases in what follows.

Assumption 1: The safety constraint (4), state constraints (6), and lateral safety constraint (7) are not active at t_i^0.

Since CAVs arrive randomly, this assumption cannot always be enforced. However, we can handle violations of Assumption 1 by foregoing optimality and simply controlling a CAV that violates it until all constraints become feasible within the CZ using the CBF method [9]. Under Assumption 1, we will start by analyzing the case of no active constraints. The analysis of the cases where one or more constraints become active is similar to the straight road merging problem studied in [5]. However, the computational time significantly increases with constrained optimal solutions.

1) Unconstrained Optimal Control: Let $\mathcal{X}_i(t) := (x_i(t), v_i(t))$ be the state vector of CAV i and $\boldsymbol{\lambda}_i(t) := (\lambda_i^x(t), \lambda_i^v(t))$ be the costate vector (for simplicity, in the sequel we omit explicit time dependence when no ambiguity arises). The Hamiltonian associated with (10) with the state constraint, control constraint and safety constraint adjoined is

$$\begin{aligned} H_i(\mathcal{X}_i, \boldsymbol{\lambda}_i, u_i) =& \frac{1}{2}u_i^2 + \beta_2\kappa(x_i)v_i^2 + \lambda_i^x v_i + \lambda_i^v u_i \\ &+ \mu_i^a(u_i - u_{max}) + \mu_i^b(u_{min} - u_i) \\ &+ \mu_i^c(v_i - v_{max}) + \mu_i^d(v_{min} - v_i) \\ &+ \mu_i^e(x_i + \varphi v_i + \delta - x_{i_p}) \\ &+ \mu_i^f(\kappa(x_i)v_i^2 - \frac{w_i^h}{h_i}g) + \beta_1. \end{aligned} \tag{11}$$

The Lagrange multipliers $\mu_i^a, \mu_i^b, \mu_i^c, \mu_i^d, \mu_i^e, \mu_i^f$ are positive when the constraints are active and become 0 when the corresponding inequalities are strict. Note that when the safety constraint (4) becomes active, i.e., $\mu_i^e > 0$, the expression above involves $x_{i_p}(t)$. When $i = 1$, the optimal trajectory is obtained without this term, since (4) is inactive over all $[t_1^0, t_1^m]$. Thus, once the solution for $i = 1$ is obtained (based on the analysis that follows), x_1^* is a given function of time and available to $i = 2$. Based on this information, the optimal trajectory of $i = 2$ is obtained. Similarly, all subsequent optimal trajectories for $i > 2$ can be recursively obtained based on $x_{i_p}^*(t)$ with $i_p = i - 1$.

An optimal control solution can now be obtained using standard Hamiltonian analysis [11]. We omit details which can be found in [3] and show the final result:

$$u_i^*(t) = \sqrt{2\beta_2\hat{\kappa}}(b_i e^{\sqrt{2\beta_2\hat{\kappa}}t} - c_i e^{-\sqrt{2\beta_2\hat{\kappa}}t}), \tag{12}$$

$$v_i^*(t) = b_i e^{\sqrt{2\beta_2\hat{\kappa}}t} + c_i e^{-\sqrt{2\beta_2\hat{\kappa}}t} - \frac{a_i}{2\beta_2\hat{\kappa}}, \tag{13}$$

$$x_i^*(t) = \frac{1}{\sqrt{2\beta_2\hat{\kappa}}}(b_i e^{\sqrt{2\beta_2\hat{\kappa}}t} - c_i e^{-\sqrt{2\beta_2\hat{\kappa}}t}) - \frac{a_i}{2\beta_2\hat{\kappa}}t + d_i, \tag{14}$$

where a_i, b_i, c_i, d_i are integration constants to be evaluated along with the optimal merging time t_i^m. Omitting details, these are obtained from the following five nonlinear algebraic equations to get a_i, b_i, c_i, d_i and t_i^m:

$$\begin{aligned} & b_i e^{\sqrt{2\beta_2\hat{\kappa}}t_i^0} + c_i e^{-\sqrt{2\beta_2\hat{\kappa}}t_i^0} - \frac{a_i}{2\beta_2\hat{\kappa}} = v_i^0, \\ & \frac{1}{\sqrt{2\beta_2\hat{\kappa}}}(b_i e^{\sqrt{2\beta_2\hat{\kappa}}t_i^0} - c_i e^{-\sqrt{2\beta_2\hat{\kappa}}t_i^0}) - \frac{a_i}{2\beta_2\hat{\kappa}}t_i^0 + d_i = 0, \\ & \frac{1}{\sqrt{2\beta_2\hat{\kappa}}}(b_i e^{\sqrt{2\beta_2\hat{\kappa}}t_i^m} - c_i e^{-\sqrt{2\beta_2\hat{\kappa}}t_i^m}) - \frac{a_i}{2\beta_2\hat{\kappa}}t_i^m + d_i = L, \\ & \sqrt{2\beta_2\hat{\kappa}}(b_i e^{\sqrt{2\beta_2\hat{\kappa}}t_i^m} - c_i e^{-\sqrt{2\beta_2\hat{\kappa}}t_i^m}) = 0, \\ & \beta_1 + \beta_2\hat{\kappa}(b_i e^{\sqrt{2\beta_2\hat{\kappa}}t_i^m} + c_i e^{-\sqrt{2\beta_2\hat{\kappa}}t_i^m} - \frac{a_i}{2\beta_2\hat{\kappa}})^2 \\ & \qquad + a_i(b_i e^{\sqrt{2\beta_2\hat{\kappa}}t_i^m} + c_i e^{-\sqrt{2\beta_2\hat{\kappa}}t_i^m} - \frac{a_i}{2\beta_2\hat{\kappa}}) = 0. \end{aligned} \tag{15}$$

Note that when $\beta_2 \to 0$ the optimal control (12) degenerates to the case without any comfort consideration. In other words, the optimal control (12) is in a simple linear form as in [5].

The equations in (15) are usually hard to solve as there are too many exponential terms (it usually takes about one second using *solve* in Matlab). This motivates us to use a computationally efficient solution which is omitted here but can be found in [3].

2) Constrained Optimal Control: When one or more constraints in the merging problem becomes active, we can use the standard interior point analysis [11] for determining all constrained arcs in an optimal trajectory and the time instants they start, similar to the straight-road merging case with no comfort constraints shown in [5]. This leads to a complete constrained optimal control solution. However, this solution can become complicated when two or more constraints become active in an optimal trajectory and very time-consuming to obtain, hence possibly prohibitive for real-time implementation. It is for this reason that we resort to the CBF method to guarantee the satisfaction of all constraints while sacrificing some performance if some constraints become active.

III. Joint Optimal Control and Control Barrier Functions (OCBF)

We briefly review the OCBF approach detailed in [9] as it applies to our merging problem. The OCBF controller aims to track the OC solution (12)-(14) while satisfying all constraints (4), (27), and (6) without solving the original constrained problem. This is accomplished by replacing each of the constraints (4), (27), (6) and (7) by a simpler one enforced by a CBF as explained next.

Consider an affine control system of the general form

$$\dot{\boldsymbol{x}} = f(\boldsymbol{x}) + g(\boldsymbol{x})\boldsymbol{u} \tag{16}$$

where $\boldsymbol{x} \in X \subset \mathbb{R}^n$, where X is a closed state constraint set, $f : \mathbb{R}^n \to \mathbb{R}^n$ and $g : \mathbb{R}^n \to \mathbb{R}^{n\times q}$ are Lipschitz continuous, and $\boldsymbol{u} \in U \subset \mathbb{R}^q$ is a closed control constraint set defined as

$$U := \{\boldsymbol{u} \in \mathbb{R}^q : \boldsymbol{u}_{min} \le \boldsymbol{u} \le \boldsymbol{u}_{max}\}. \tag{17}$$

with $\boldsymbol{u}_{min}, \boldsymbol{u}_{max} \in \mathbb{R}^q$ and the inequalities are interpreted componentwise.

Given a constraint $b(\boldsymbol{x}) \geq 0$, the function b is a *Control Barrier Function* (CBF) if there exists a class $\mathcal{K}$ function α_1 (i.e., it is strictly increasing and $\alpha(0) = 0$) such that for all $x \in C := \{\boldsymbol{x} \in \mathbb{R}^n : b(\boldsymbol{x}) \geq 0\}$,

$$\sup_{\boldsymbol{u} \in U} [L_f b(\boldsymbol{x}) + L_g b(\boldsymbol{x}) \boldsymbol{u} + \alpha_1(b(\boldsymbol{x}))] \geq 0, \qquad (18)$$

where L_f, L_g denote the Lie derivatives of $b(\boldsymbol{x})$ along f and g respectively. It has been established (e.g., [3], [12]), that if $\boldsymbol{x}(0) \in C$, then any Lipschitz continuous controller $\boldsymbol{u}(t)$ that satisfies (18) for all $t \geq 0$ renders C forward invariant for system (16). In simple terms, any control satisfying (18) is guaranteed to satisfy the original constraint $b(\boldsymbol{x}) \geq 0$.

The above holds under the assumption that $L_g b(\boldsymbol{x}) \neq 0$ when $b(\boldsymbol{x}) = 0$. If this condition does not hold, we extend the definition of a CBF to that of a *High Order Control Barrier Function* (HOCBF) as follows. For a constraint $b(\boldsymbol{x}) \geq 0$ with relative degree m, $b : \mathbb{R}^n \to \mathbb{R}$, and $\psi_0(\boldsymbol{x}) := b(\boldsymbol{x})$, we define a sequence of functions $\psi_i : \mathbb{R}^n \to \mathbb{R}, i \in \{1, \ldots, m\}$:

$$\psi_i(\boldsymbol{x}) := \dot{\psi}_{i-1}(\boldsymbol{x}) + \alpha_i(\psi_{i-1}(\boldsymbol{x})), i \in \{1, \ldots, m\}, \quad (19)$$

where $\alpha_i(\cdot)$, $i \in \{1, \ldots, m\}$, denotes a $(m-i)^{th}$ order differentiable class $\mathcal{K}$ function. We further define a sequence of sets C_i, $i \in \{1, \ldots, m\}$, associated with (19) in the form:

$$C_i := \{\boldsymbol{x} \in X : \psi_{i-1}(\boldsymbol{x}) \geq 0\}, i \in \{1, \ldots, m\}. \qquad (20)$$

Then, a function $b : \mathbb{R}^n \to \mathbb{R}$ is a HOCBF of relative degree m for system (16) if there exist $(m-i)^{th}$ order differentiable class $\mathcal{K}$ functions $\alpha_i, i \in \{1, \ldots, m-1\}$ and a class $\mathcal{K}$ function α_m such that

$$\sup_{\boldsymbol{u} \in U} [L_f^m b(\boldsymbol{x}) + L_g L_f^{m-1} b(\boldsymbol{x}) \boldsymbol{u} + R(b(\boldsymbol{x})) + \alpha_m(\psi_{m-1}(\boldsymbol{x}))] \geq 0 \qquad (21)$$

for all $\boldsymbol{x} \in C_1 \cap, \ldots, \cap C_m$. where it is assumed that $L_g L_f^{m-1} b(\boldsymbol{x}) \neq 0$ when $b(\boldsymbol{x}) = 0$.

In addition, a *Control Lyapunov Function* (CLF) is a continuously differentiable function $V : \mathbb{R}^n \to \mathbb{R}$ for system (16) if there exist constants $c_1 > 0, c_2 > 0, c_3 > 0$ such that for all $\boldsymbol{x} \in \mathbb{R}^n$, $c_1 ||\boldsymbol{x}||^2 \leq V(\boldsymbol{x}) \leq c_2 ||\boldsymbol{x}||^2$,

$$\inf_{\boldsymbol{u} \in U} [L_f V(\boldsymbol{x}) + L_g V(\boldsymbol{x}) \boldsymbol{u} + c_3 V(\boldsymbol{x})] \leq 0. \qquad (22)$$

It is common to combine CBFs for systems with relative degree one with quadratic costs to form optimization problems. A solution to such problems can be obtained by discretizing time and a Quadratic Program (QP) is solved at each time step subject to constraints of the form (21). If convergence to a state is desired, then a CLF constraint of the form (22) is added to the QP. The optimal control obtained by solving each QP is applied at the current time step and held constant for the whole interval. The state is updated using dynamics (16), and the procedure is repeated.

Along these lines, the OCBF controller solves the following problem:

$$\min_{u_i(t), e_i(t)} J_i(u_i(t), e_i(t)) = \int_{t_i^0}^{t_i^m} \left(\beta e_i^2(t) + \frac{1}{2} (u_i(t) - u_{ref}(t))^2 \right) dt \qquad (23)$$

subject to the CBF constraints, each obtained by applying (18) or (21) that enforce (4), (6), (27), and (7), and to the CLF constraint for tracking. Here, $\beta > 0$ and $e_i(t)$ is a relaxation variable in the CLF constraint. The obvious selection for the control (acceleration) reference signal is $u_{ref}(t) = u_i^*(t)$ given by (12). However, we can improve the tracking process using $x_i^*(t)$ from (14) by selecting instead:

$$u_{ref}(t) = \frac{x_i^*(t)}{x_i(t)} u_i^*(t). \qquad (24)$$

Alternative choices of $u_{ref}(t)$ are also possible as shown in [13], [9].

Deriving the CBF constraint for the safe merging constraint (27) poses a technical challenge due to the fact that it only applies at a certain time t_i^m, whereas a CBF is required to be in a continuously differentiable form. To tackle this problem, a technique used in [3] is applied to convert (27) to a continuous differentiable form as follows:

$$z_{i,i_c}(t) - \Phi(x_i(t)) v_i(t) - \delta \geq 0, \quad \forall t \in [t_i^0, t_i^m], \qquad (25)$$

where i_c is the index of the CAV that conflicts with i determined by some sequencing policy, the simplest case being FIFO as in the previous section (i.e., $i_c = i - 1$). The function $\Phi : \mathbb{R} \to \mathbb{R}$ may be chosen to be any continuously differentiable function as long as it is strictly increasing and satisfies the boundary conditions $\Phi(x_i(t_i^0)) = 0$ and $\Phi(x_i(t_i^m)) = \varphi$. In this case, a linear function can satisfy both conditions: $\Phi(x_i(t)) = \varphi \frac{x_i(t)}{L}$ where L is the length of road traveled by the CAV from its entry to the CZ to the MP of interest in (27).

We refer to the resulting control $u_i(t)$ in (23) as the "OCBF control". The solution to (23) is obtained through the method outlined above: we discretize the time interval $[t_i^0, t_i^m]$ with time steps of length Δ and solve (23) over $[t_i^0 + k\Delta, t_i^0 + (k+1)\Delta]$, $k = 0, 1, \ldots$, with $u_i(t), e_i(t)$ as decision variables held constant over each such interval. Consequently, each such problem is a QP since we have a quadratic cost and a number of linear constraints on the decision variables at the beginning of each interval. The solution of each such problem gives $u_i^*(t_i^0 + k\Delta)$, $k = 0, 1, \ldots$, allowing us to update (1) in the k^{th} time interval. This process is repeated until CAV i leaves the CZ.

A. Simulation Results for Traffic Merging Control

To illustrate the OCBF approach, we have selected a merging configuration that occurs in the US interstate highway I-90 (known as the Massachusetts Turnpike) in the Boston area, which is similar to Fig. 1. An exact map and details can be found in [3]. Here, we provide a summary of the results in Table I to compare the preformance of the OCBF controller to a baseline consisting entirely of human-driven vehicles based on the Vissim microscopic multi-model traffic flow simulation tool employing a standard car-following model [14] that simulates human psycho-physiological driving behavior. Since we choose different α_1, α_2 parameters for the main and merging roads, we list the metrics separately in this table.

TABLE I: Objective function comparison

Rate(CAVs/h)	Main:500, Merg.:500			Main:500, Merg.:800		
Method	Vissim	OCBF	DR	Vissim	OCBF	DR
Main time (s)	22.27	13.35	12.49	22.43	15.57	13.30
Main comfort	9.07	15.75	16.71	9.03	13.46	15.72
Main $\frac{1}{2}u_i^2(t)$	1.21	10.93	10.42	1.23	12.86	14.35
Main obj.	92.76	72.42	69.22	93.37	81.43	75.63
Merg. time (s)	26.71	15.92	15.94	39.02	16.40	16.32
Merg. comfort	35.89	50.77	50.73	30.61	49.50	49.75
Merg. $\frac{1}{2}u_i^2(t)$	13.78	0.05	1.13	13.29	1.79	3.20
Merg. obj.	301.3	238.4	239.6	606.6	241.0	242.3

When the traffic rates in the main and merging roads are equal at 500 CAVs/h, the overall objective function of CAVs in the main road improves about 22% with the OCBF method (using FIFO) compared with Vissim, and it further improves about 4% with the OCBF method when a dynamic resequencing method (see [15]) is used as an alternative to FIFO. Observe that when the traffic arrival rate increases to 1000 CAVs/h for both the main and merging roads, the human driven vehicles in the merging road will cause a heavy traffic congestion in Vissim, while the OCBF method can successfully manage the traffic without any congestion at all

IV. Optimal Control of Autonomous Vehicles in Mixed Traffic with Safety Guarantees

In mixed traffic, CAVs must co-exist with Human Driven Vehicles (HDVs) whose behavior is unpredictable and possibly uncooperative. Still, however, a CAV must operate so as to guarantee safety, i.e., satisfy the same constraints as in the previous section.

We begin by partitioning the index set of all vehicles $F(t)$ by defining: $F_C(t)$ containing the indices associated with CAVs in the CZ, and $F_H(t)$ containing the indices of HDVs in the CZ at time t (i.e., $F_C(t) \cup F_H(t) = F(t)$). Similarly, let $F_1(t)$ and $F_2(t)$ be the sets of indices of all vehicles inside the CZ at time t in roads 1, 2 respectively (i.e. $F_1(t) \cup F_2(t) = F(t)$). Along with the cardinality $N(t)$ f $F(t)$, we define $N_H(t)$, $N_C(t)$, $N_1(t)$ and $N_2(t)$ to be the cardinalities of $F_H(t)$, $F_C(t)$, $F_1(t)$ and $F_2(t)$ respectively.

The safe merging constraint in (27) is rewritten as

$$z_{i,i^+}(t_i^m) - \varphi v_i(t_i^m) - \delta \geq 0, \tag{26}$$

where $i^+ \in F(t)$ is the index of the vehicle (CAV or HDV) that may collide with CAV i at the MP. The determination of i^+ depends on the driving behavior of HDVs and the policy adopted for sequencing CAVs through the CZ. In order to express this in a continuously differentiable form amenable to a CBF constraint, we use the same technique as in (25) and write

$$z_{i,i^+}(t) - \Phi\big(x_i(t)\big)v_i(t) - \delta \geq 0, \tag{27}$$

Mixed traffic requires an additional safe merging constraint due to uncooperative HDVs. In particular, let i^- be the vehicle that CAV i has to merge ahead of. Therefore, there has to have enough space for CAV i to safely merge ahead of i^-, i.e.,

$$z_{i^-,i}(t_i^m) - \varphi v_{i^-}(t_i^m) - \delta \geq 0. \tag{28}$$

This new constraint ensures that the trailing HDV (if present) has enough space to avoid any collision; otherwise, CAV i cannot merge ahead of it and must yield. Note that if $i^- \in F_C(t)$ this constraint is rendered redundant as CAV i is already a safe merging constraint for CAV i^-. Similar to (27), we transform this constraint to obtain:

$$z_{i^-,i}(t) - \Phi\big(x_{i^-}(t)\big)v_{i^-}(t) - \delta \geq 0. \tag{29}$$

A. Safe Sequencing

Although First In First Out (FIFO) is a popular sequencing policy that performs well in symmetric merging with 100% CAV traffic, such *fixed* policies may fail in mixed traffic since HDVs are not guaranteed to conform to such a policy. The *Shortest Distance First* (SDF) policy is used to find candidates for i^+ and i^- introduced earlier. They are called "candidates" since the unpredictability of HDV behavior cannot ensure safe merging under this policy. The purpose of an upper-level controller, before using a lower-level motion controller for each CAV, is to derive instead a *Safe Sequencing* (SS) policy derived from SDF. At every time step t, the coordinator determines a *safe* (precisely defined below) merging sequence in a centralized manner. This is accomplished in the following steps.

Step 1: Generate the SDF sequence. The SDF sequence is defined at t, denoted by $\boldsymbol{s}^0(t)$ (t will be henceforth omitted for simplicity), as the sequence of vehicles such that all $i, j \in F(t)$ satisfy $L - x_i(t) < L - x_j(t) \Leftrightarrow \boldsymbol{s}^0(i) < \boldsymbol{s}^0(j)$, where $\boldsymbol{s}^0(i)$ denotes the position of i in the sequence and $L - x_i(t)$ is the remaining distance of car i from the MP. For any $i \in \boldsymbol{s}^0$, one can identify i^+ and i^- for i as in (26), (28) and, for the SDF sequence, denote these by $\hat{\imath}^+$ and $\hat{\imath}^-$. Let $\text{ind}[\boldsymbol{s}^0(i)]$ denote the index of the vehicle at position $\boldsymbol{s}^0(i)$ in $\boldsymbol{s}^0$:

$$\hat{\imath}^- = \min_{j>0}\Big\{\text{ind}[\boldsymbol{s}^0(i)+j]\Big\} \text{ s.t. } i \in F_r \Rightarrow \text{ind}\big[\boldsymbol{s}^0(i)+j\big] \in F_{\bar{r}} \tag{30}$$

$$\hat{\imath}^+ = \min_{j>0}\Big\{\text{ind}[\boldsymbol{s}^0(i)-j]\Big\} \text{ s.t. } i \in F_r \Rightarrow \text{ind}\big[\boldsymbol{s}^0(i)-j\big] \in F_{\bar{r}} \tag{31}$$

Step 2: Generate safe sequences. In the presence of HDVs, the SDF sequencing policy can lead to safety issues: (i) there is no assumption on the HDV behavior which may not be cooperative, and (ii) even if cooperation is assumed, there is no way to ensure the vehicles follow the SDF policy since they are on different roads and may not detect each other. Therefore, one way to prevent this problem is for CAV i to *always merge ahead of another CAV*, i.e., set $i^- \in F_C(t)$. However, this may be overly conservative since there are cases when $i^- \in F_H(t)$ but the relative distance from the MP between the HDV and CAV is positive and large. In this case, yielding to make room for the HDV at the MP is excessively conservative. This can be avoided by incorporating a distance threshold in the determination of i^-

and i^+. The feasible set for i^+, i^- therefore can be extended to $\{\text{CAV}, \text{HDV}, \emptyset\}$ for all $i \in F_C^{SZ}(t)$ where $\{\emptyset\}$ signifies that there is no vehicle within the preset threshold; in other words, if $i^- = \emptyset$, then CAV i is unconstrained in planning an optimal merging trajectory and needs to only consider i^+. This is formalized as follows.

Merging pair determination: Recalling the safe merging constraints (27), (29), one can define $\Delta_i^-(j) = x_i(t) - x_j(t) - \Phi\big(x_j(t)\big)v_j(t) - \delta$ and $\Delta_i^+(j) = x_j(t) - x_i(t) - \Phi\big(x_i(t)\big)v_i(t) - \delta$. As long as $\Delta_i^-(j) < 0$, we use $\hat{i}^-$ from (30) as i^-; otherwise $i^- = \emptyset$. The same applies to i^+ and we have:

$$i^- = \begin{cases} \hat{i}^- & \text{if } \Delta_i^-(\hat{i}^-) < 0, \\ \emptyset & \text{otherwise,} \end{cases}, \quad i^+ = \begin{cases} \hat{i}^+ & \text{if } \Delta_i^+(\hat{i}^+) < 0, \\ \emptyset & \text{otherwise,} \end{cases} \tag{32}$$

We can now define a *Safe sequence* to be a merging sequence of i if $i^- \in \{CAV, \emptyset\}$ for all $i \in F_C^{SZ}(t)$. Thus, in a safe sequence, if a CAV that merges ahead of another CAV their mutual cooperation ensures safe merging; if $i^- = \emptyset$, then any vehicle following i is located further than the preset threshold (32) and (27) can be satisfied to ensure safe merging. Using this definition, at the conclusion of **Step 2** a set safe sequences $\mathcal{S}_S$ is generated.

Step 3: Generate minimally disruptive safe sequences. It is likely that the set $\mathcal{S}_S$ contains multiple safe sequences. In order to differentiate among them, the concept of *disruption*, can be introduced as follows:

$$D(\boldsymbol{s}, \boldsymbol{s}^0) = \sum_{i=1}^{N(t)} \mathbf{1}\big[\boldsymbol{s}(i) \neq \boldsymbol{s}^0(i)\big], \tag{33}$$

where $D(\boldsymbol{s}, \boldsymbol{s}^0)$ measures the disruption caused by a safe sequence $\boldsymbol{s}$ relative to the SDF sequence $\boldsymbol{s}^0$ as one with the least number of changes in indices compared to $\boldsymbol{s}^0$ ($\mathbb{1}(\cdot)$ is the indicator function). Thus, the subset of safe sequences with minimal disruption is determined by $\mathcal{S}_O = \operatorname{argmin}_{\boldsymbol{s} \in \mathcal{S}_S} D(\boldsymbol{s}, \boldsymbol{s}^0)$.

Step 4: Determine the optimal safe sequence $\boldsymbol{s}_F$. If $|\mathcal{S}_O| = 1$, the optimal safe sequence is obtained in **Step 3**. If $|\mathcal{S}_O| > 1$, then the sequence $\boldsymbol{s}_F$ is chosen such that gives higher priority to vehicles located on road $r \in \{1, 2\}$ with higher average velocity. Let r_1 be the road with a higher average velocity, the optimal safe sequence is as follows:

$$\boldsymbol{s}_F = \operatorname*{argmin}_{\boldsymbol{s} \in \mathcal{S}_O} \left(\sum_{i \in F_{r_1}} i - \sum_{j \notin F_{r_1}} j \right). \tag{34}$$

Two properties can be established for the safe sequences: (i) The optimal safe sequence $\boldsymbol{s}_F$ satisfies all original rear-end safety constraints. (ii) There always exists a safe sequence $\boldsymbol{s}_S$, $\boldsymbol{s}_S = \{\boldsymbol{s}^0 i^+, i^- F_{\bar{r}}^{SZ}, i F_r^{SZ}\}$.

Once a safe sequence is determined, the optimal motion control can be carried out exactly as in Section III simply using the value of i_c in (25) which is obtained through the safe sequence whose construction was described above.

The concept of a safe sequence can be extended to all CZs in a traffic network. In some cases, it can be shown (see [16] that such a safe sequence is actually optimal (compared to a CAV merging ahead of a HDV rather than another CAV) which renders the unpredictable human driver irrelevant. More generally, a mixed traffic environment can be viewed as a multi-player game where some players (CAVs) are cooperative and others (HDVs) are not. Depending on the situation, a set of cooperative players can form a *coalition* that induces one or more uncooperative players to behave in a manner that optimizes a given system-wide objective. In [16], this is shown for the problem of highway lane changing where two CAVs (one in the fast and the other in the slow lane) to cooperate to allow one to optimally change lanes with guaranteed safety.

While mixed traffic environments present significant challenges to traffic control compared to the 100% CAV setting, they also offer some novel opportunities as discussed in the next section.

V. Learning-based Control of Mixed-Autonomy Traffic

In the previous section, we saw how cooperation among CAVs in mixed traffic provides opportunities to induce desirable behavior for HDVs and ensure safety in conflict areas. More broadly, the presence of CAVs enables new traffic control paradigms. Classical traffic control is often based on sensors fixed in the road infrastructure to measure vehicle densities and flows with control actuation implemented through digital speed signs [17], [18]. Mobile communication technology allows CAVs to act as probe vehicles observing the state of traffic in their surroundings. At the same time, CAVs can also act as actuators as their velocity can be automatically regulated in the future. In this section, we first outline the control architecture for such a traffic control paradigm, which was recently introduced in the literature. The method of estimating the traffic state from probe vehicle data is then described followed by an illustration of a control law to dissipate traffic congestion.

A. Lagrangian Traffic Control Architecture

A traffic control architecture based on CAV mobile sensing and actuation is detailed in Fig. 2. The control objective is to reduce traffic congestion by smoothing the vehicle flow. Flow and density measurements from a few CAVs (red vehicles) are used to learn a traffic model for the rest of the vehicles (blue). One such classical model is the Lighthill-Whitham-Richards (LWR) PDE

$$\frac{\partial \rho(x,t)}{\partial t} + \frac{\partial V(\rho(x,t))\rho(x,t)}{\partial x} = 0,$$

which describes how the vehicle density $\rho = \rho(x,t)$ varies over space x and time t [19], [20]. Here, $V(\rho)$ represents how traffic flow depends on density. The velocity of individual CAVs can be modeled by the ODEs

$$\dot{x}_i(t) = V(\rho(t, x_i(t))), \quad i = 1, \ldots, N,$$

where N is the number of CAVs considered in a given scenario. The traffic system to be controlled is consequently governed by a coupled system of PDEs and ODEs, which

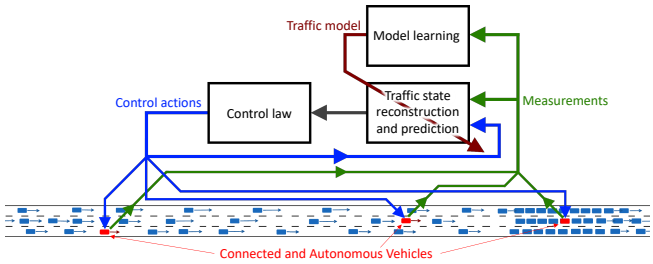

Fig. 2: Lagrangian traffic control architecture. CAVs are used to gather traffic state information and to implement control actions. The controller is based on a machine learning model enabling the prediction of the future traffic state, which is utilized by the control law. Illustration adopted from [23].

pose significant mathematical challenges [21], [22]. Because the traffic control is based on mobile sensors and actuators, it is sometimes referred to as Lagrangian traffic control because of the similarity to Lagrange's model of fluid.

The traffic model learned from CAV data is used to reconstruct the traffic state throughout the considered road segment, also for portions where no CAVs have been driving. The model and reconstructed state form the basis of the traffic state prediction. Like the scenario in Fig. 2, this can mean predicting the evolution of the high-density area to the right. Based on the prediction, the controller computes the receding-horizon control actions for the CAVs to mitigate the congestion by potentially slightly slowing down some of the CAVs.

B. Learning-based Traffic State Estimation

Let us next discuss in some more detail how the above traffic model can be learned using physics-informed neural networks [24] as proposed in [25], [26].

We modify the original LWR model by adding the second-order term $\gamma^2\partial^2\rho/\partial x^2$ to the right-hand side, obtaining a "diffusively corrected" LWR. This model is learned using sampled measurements $\{x_i(t), \rho_i(t), V_i(t)\}$ from probe vehicles $i = 1, \dots, N$. The goal is to obtain a model for the density $\hat{\rho}^\star = \arg\min_{\hat{\rho}} \int_0^T \|\rho(t,\cdot) - \hat{\rho}(t,\cdot)\|^2 dt$. We do that by using feedforward neural networks to represent the maps $\hat{\rho}_{\Theta_\rho} = \hat{\rho}_{\Theta_\rho}(t,x)$ and $\hat{V}_{\Theta_V} = V_{\Theta_V}(\rho)$, where Θ_ρ and Θ_V denote the parameters of the networks. To tune the parameters, the following optimization problem is considered

$$\min_{\Theta_\rho,\Theta_V} \frac{1}{N}\sum_{i=1}^{N}\int_0^T \Big\{|\hat{\rho}_{\Theta_\rho}(t,x_i(t)) - \rho_i(t)|^2 + |\hat{V}_{\Theta_V}(\rho_i(t)) - V_i(t)|^2\Big\} dt$$

$$\text{s.t.} \quad \frac{\partial\hat{\rho}_{\Theta_\rho}}{\partial t} + \frac{\partial\hat{V}_{\Theta_V}(\hat{\rho}_{\Theta_\rho})\hat{\rho}_{\Theta_\rho}}{\partial x} = \gamma^2\frac{\partial^2\hat{\rho}_{\Theta_\rho}}{\partial x^2}$$

$$\left|\frac{\partial\hat{V}_{\Theta_V}}{\partial\rho}(\rho)\right|_+ = 0,$$

where the constraints impose the desired physical properties of the traffic model. Through Lagrangian relaxation, we obtain the optimization problem

$$\begin{aligned}\min_{\Theta_\rho,\Theta_V}\max_{\lambda_\rho,\lambda_V} \frac{1}{N}\sum_{i=1}^{N}\int_0^T &\Big\{|\hat{\rho}_{\Theta_\rho}(t,x_i(t)) - \rho_i(t)|^2 \\ &+ |\hat{V}_{\Theta_V}(\rho_i(t)) - V_i(t)|^2\Big\} dt \\ &+ \lambda_\rho \iint_{[0,T]\times[0,L]} \left|\frac{\partial\hat{\rho}_{\Theta_\rho}}{\partial t}(\nu) + \frac{\partial\hat{V}_{\Theta_V}(\hat{\rho}_{\Theta_\rho})\hat{\rho}_{\Theta_\rho}}{\partial x}(\nu) \right. \\ &\qquad \left. - \gamma^2\frac{\partial^2\hat{\rho}_{\Theta_\rho}}{\partial x^2}(\nu)\right| d\nu \\ &+ \lambda_V \int_0^1 \left|\frac{\partial\hat{V}_{\Theta_V}}{\partial\rho}(\rho)\right|^2 d\rho \\ =: \min_{\Theta_\rho,\Theta_V}\max_{\lambda_\rho,\lambda_V} &\mathcal{L}_{\lambda_\rho,\lambda_V}(\Theta_\rho,\Theta_V).\end{aligned}$$

This problem can be solved numerically by primal-dual gradient descent iterations based on the primal problem

$$\Theta_\rho^*(\lambda_\rho), \Theta_V^*(\lambda_V) = \arg\min_{\Theta_\rho,\Theta_V} \mathcal{L}_{\lambda_\rho,\lambda_V}(\Theta_\rho,\Theta_V)$$

and the dual problem

$$\lambda_\rho^*(\Theta_\rho), \lambda_V^*(\Theta_V) = \arg\max_{\lambda_\rho,\lambda_V} \mathcal{L}_{\lambda_\rho,\lambda_V}(\Theta_\rho,\Theta_V).$$

See [25] for further details on the implementation.

Fig. 3 shows how the density ρ depends on t and x for a scenario simulated in SUMO [27]. Seven minutes over two and a half kilometers are presented. Fig. 3(a) illustrates how the vehicle density varies between high (red) and low (blue) with black curves indicating how individual CAVs drive through the road segment. Note that when the density is lower the CAVs drive faster, and when the CAVs experience congestion they drive slower, as expected from the traffic model. Based on samples obtained by CAVs in Fig. 3(a), Fig. 3(b) shows the reconstructed traffic state using the physics-informed machine learning approach described above. Despite the sparse sampling of the spatial-temporal domain by the CAVs, the estimated traffic density in Fig. 3(b) is close to the true one in Fig. 3(a).

C. Vehicle Control to Dissipate Traffic Congestion

Vehicles moving slower than the average traffic act as moving bottlenecks slowing other vehicles [22], [28]–[30]. By actively controlling the CAVs it is thus possible to slightly reduce or increase the traffic flow, and thereby influence traffic congestion downstream. Fig. 4 shows this situation, where a car accident happens at 50 km at time t_0. The accident gives rise to high density (yellow area), propagating backward in space. In Fig. 4(a), the red curve indicates a CAV driving at constant speed (straight line) until it reaches the congested area (yellow) when it slows down. After the congested area, it continues with a higher constant speed again. The size of the congested area corresponds to the severity of the accident in the sense of how much it influences the travel time for general traffic. Using the estimated and predicted traffic status, it is possible to slow down the CAV to reduce the congested area. Fig. 4(b) shows a situation where the controller does

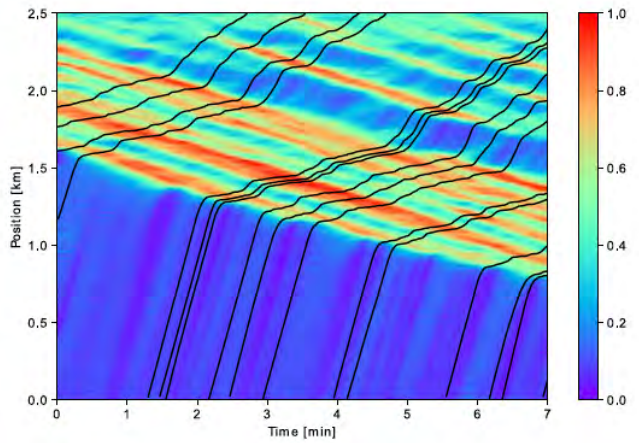

(a)

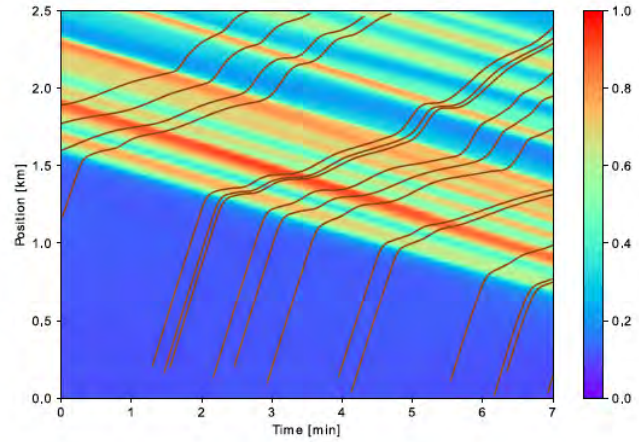

(b)

Fig. 3: (a) Simulated traffic over a 2.5 km road segment. The color indicates vehicle density, for instance, the red areas have high density. The black curves are the trajectories of CAVs. (b) Estimated densities based on collected CAV data using the described physics-informed machine learning approach. The estimated density agree quite well with the true density. Numerical results of [25].

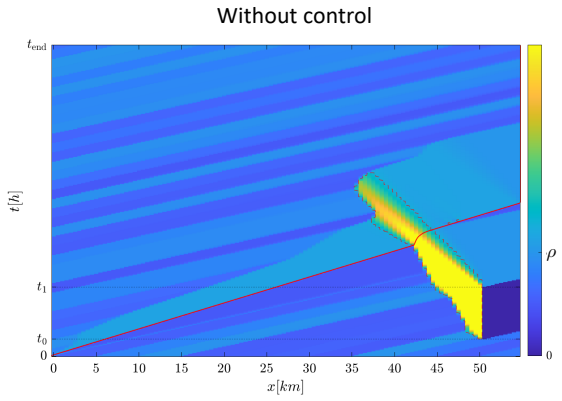

(a)

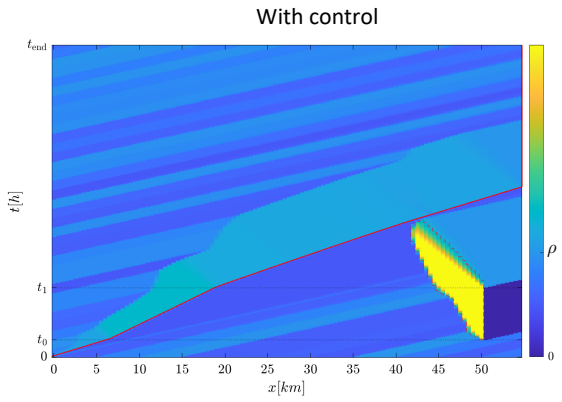

(b)

Fig. 4: (a) A CAV (red curve) driving through a highly congested area indicated by the yellow region. (b) By controlling the velocity of the CAV, it is possible to reduce the traffic flow into the congested area and thereby mititage the influece of the congestion on the total travel time for all the vehicles driving through the considered road segment. Numerical results of [29].

that, as follows from the fact that the slope of the red curve is slightly larger. Note that the slowdown of the CAV leads to that the density behind the CAV is slightly higher in Fig. 4(b) compared to Fig. 4(a), and as a consequence the (yellow) congested area is reduced in Fig. 4(b). It can be shown that the overall vehicle travel time in this scenario is significantly reduced thanks to CAV control [29], [31], so CAV traffic control provides societal benefits.

VI. Mobility Equity in Emerging Mobility Systems

The preceding sections have focused on the optimization and control of emerging mobility systems, addressing objectives such as minimizing travel time, maximizing energy efficiency, and ensuring safety in both autonomous and mixed traffic environments. While these efforts contribute significantly to the operational effectiveness of intelligent transportation systems, they often overlook the broader societal implications—particularly the equitable distribution of mobility benefits across diverse populations.

Emerging mobility systems, including CAVs, shared mobility services, and on-demand platforms, offer the potential to alleviate congestion, reduce transportation costs, and improve sustainability. At the vehicle level, extensive research has demonstrated energy efficiency gains in various traffic scenarios, such as on-ramp merging [32], signalized [33], [34] and unsignalized intersections [35]–[38], adjacent intersections [39], [40], roundabouts [41], and urban corridors [42]–[44]. At the network level, control frameworks integrating routing and coordination have also been explored [45], [46].

Despite these advances, strategies that address societal challenges—particularly *mobility equity*—remain underdeveloped [47]. Although equity considerations have received attention in public transit systems, their integration into emerging intelligent transportation networks is still in its infancy. Much of the prior work has centered on quantifying

access to employment opportunities for various demographic groups, using either simple distance-based measures or more sophisticated formulations that incorporate travel times. Isochronic accessibility metrics [48]–[52] estimate the number of opportunities reachable within fixed time thresholds. To better reflect user experience, Mavoa et al. [53] proposed an index incorporating walking and waiting times. Alternatively, gravity-based approaches model travel time as a disutility, evaluating accessibility based on the ease of reaching services across the network [54]–[56]. El-Geneidy et al. [57] further demonstrated that including monetary costs in these models more accurately reflects mobility constraints faced by low-income individuals.

To address these gaps, we introduce a comprehensive *Mobility Equity Metric (MEM)* [58]–[60] for evaluating equity in emerging mobility systems. Central to this framework is a node-level *Mobility Index (MI)* that quantifies accessibility to essential services—such as health care, education, food, and finance—via multiple transportation modes. The MI incorporates travel times, mode-specific costs, service importance, and demographic sensitivity to cost. Accessibility is calculated using isochrone and point-of-interest (POI) data from public sources [61], enabling large-scale, low-cost evaluations. Equity is assessed by applying a population-weighted Gini coefficient to the distribution of MI values, resulting in a unified, interpretable metric that captures disparities in access across a transportation network.

A. The Mobility Equity Metric

We model the transportation network as a directed graph $\mathcal{G} = (\mathcal{V}, \mathcal{E})$, where $\mathcal{V}$ is the set of nodes and $\mathcal{E}$ the set of edges. The set $\mathcal{M}$ denotes available transportation modes (e.g., public transit, shared mobility, private vehicles, cycling, walking), and $\mathcal{S}$ represents types of accessible services. To assess mobility equity, we focus on travel to essential services—such as medical facilities, groceries, schools, and financial services—though the service set can be adapted for specific applications.

Each mode $m \in \mathcal{M}$ has an associated cost per passenger mile c_m, and each service type $s \in \mathcal{S}$ has a priority weight β^s, emphasizing essential over non-essential services. The time threshold τ_m specifies the acceptable travel time for mode m, and $\sigma^s_{i,m}(\tau_m)$ denotes the number of accessible services of type s from node i within τ_m.

The MI at node i is defined as

$$\varepsilon_i = \sum_{m \in \mathcal{M}} e^{-\kappa_i c_m} \left(\sum_{s \in \mathcal{S}} \beta^s \tilde{\sigma}^s_{i,m}(\tau_m) \right), \tag{35}$$

where κ_i captures price sensitivity, and $\tilde{\sigma}^s_{i,m}(\tau_m)$ is the normalized count of accessible services:

$$\tilde{\sigma}^s_{i,m}(\tau_m) = \frac{\sigma^s_{i,m}(\tau_m)}{\max_{v \in \mathcal{V}} \sigma^s_{v,m}(\tau_m)}. \tag{36}$$

Normalization mitigates bias toward abundant services (e.g., restaurants) and ensures a balanced evaluation across service types, even with differing priority weights. The MI integrates travel time, user cost, price sensitivity, transportation modes, and service types into a unified measure of accessibility for each node $i \in \mathcal{V}$. By weighing services according to priority, the MI remains robust to variations in included services or travel purposes. We allow the price sensitivity κ_i to vary across nodes to reflect demographic differences in ability to pay, recognizing that each node typically represents a distinct neighborhood. Thus, κ_i captures the trade-off between travel time and cost differently for each region. For instance, travelers from low-income neighborhoods may exhibit higher κ_i values, emphasizing lower-cost transportation modes such as public transit over private vehicles. Consequently, the MI serves as a measure of the *ability to move* for travelers originating from node $i \in \mathcal{V}$.

To evaluate the MI for any node $i \in \mathcal{V}$ within a transportation network, we must first compute the number of accessible services $\sigma^s_{i,m}(\tau_m)$ of each type $s \in \mathcal{S}$ using each mode $m \in \mathcal{M}$. To achieve this, we leverage publicly available isochrone data. Each isochrone is a polygon surrounding a node i that captures the boundary of the geographic area that can be accessed using mode m within a time threshold τ_m.

We utilize a publicly available POI dataset to collect the numbers of services of various types within different regions. Each POI datum contains the geographic location of a specific service and its service type. By superimposing this data onto the isochrones, we can count the number of accessible services from a node $i \in \mathcal{V}$ within specific time frames. Figure 5 visualizes the distribution of essential and non-essential services within an isochrone for each mode of transportation. The points represent different service locations, with color variations indicating the types of services. Essential services, such as medical facilities and schools, are marked in distinct colors, emphasizing their significance in evaluating mobility equity.

While the MI quantifies accessibility and mobility costs at each network node, evaluating equity requires assessing the distribution of MI values across nodes. We define the MEM using a Gini coefficient modified to account for population. Given the MI for each node $i \in \mathcal{V}$ of graph $\mathcal{G}$, the MEM is

$$\mathrm{MEM}(\mathcal{G}) = 1 - \frac{\sum_{i \in \mathcal{V}} \sum_{j \in \mathcal{V}} p_i p_j \left| \varepsilon_i - \varepsilon_j \right|}{2 (\sum_{i \in \mathcal{V}} p_i)(\sum_{i \in \mathcal{V}} p_i \varepsilon_i)}, \tag{37}$$

where p_i denotes the population at node i.

The MEM value lies in $[0, 1]$, where $\mathrm{MEM}(\mathcal{G}) = 1$ indicates perfect equity, i.e., identical MI values across all nodes. Lower values reflect greater disparities in accessibility. By incorporating node populations, the metric ensures that equity is measured with respect to travelers rather than spatial regions, mitigating biases due to uneven population distributions.

While travel demand could replace population to assess mobility equity per traveler rather than per capita, doing so introduces challenges related to data collection and biases, as current demand patterns may reflect existing mobility constraints rather than actual needs. Future advancements in mobility services and infrastructure could mitigate these limitations by enabling more accurate demand measurement. We can compute MEM using average traffic conditions and

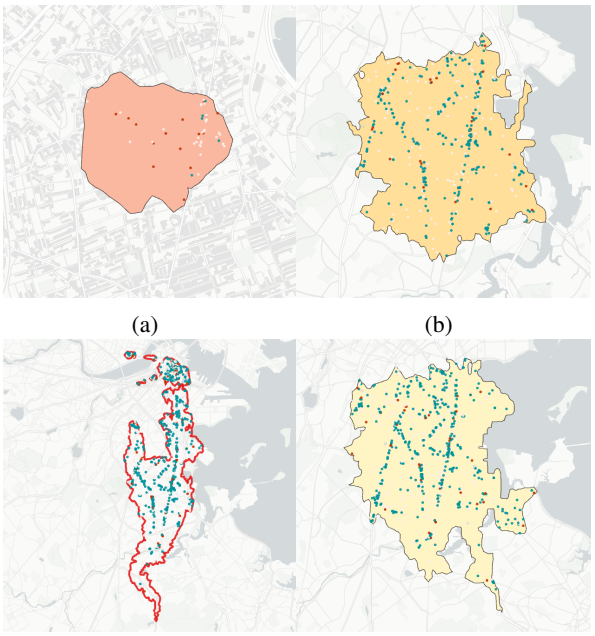

(a) (b) (c) (d)

Fig. 5: Illustration of accessible services within the isochrone for each mode of transportation: (a) walking, (b) bicycle, (c) public transit, (d) driving.

TABLE II: Priority level of services

Service Type	β	Service Type	β
Cafe	1/23	Restaurant	2/23
Fitness	2/23	School	3/23
Hospital	3/23	Stadium	1/23
Market	3/23	Theater	1/23
Park	2/23	Place of Worship	2/23
Pharmacy	3/23	-	-

static coefficients to highlight structural inequities. However, the framework can be extended to incorporate temporal variations. When time-specific isochrone data are available, MEM can be evaluated separately across different periods (e.g., peak hours, off-peak hours, weekends) to capture temporal dynamics. Additionally, time-varying price sensitivities could be incorporated. Such extensions would reveal how mobility inequities evolve throughout the day and week.

B. Implementation of the Mobility Equity Metric

In this subsection, we demonstrate the applicability of the proposed MEM through an analysis of mobility equity across 12 major U.S. cities. Each city is divided into communities based on census tract data [62]. Using demographic information, we evaluate the MI for each community by considering accessibility to eleven essential services from the centroid of each community and accounting for residents' average income levels.

We collect POI data using the TOMTOM API [63] to geolocate services and generate isochrones from each community centroid for walking, bicycling, public transit, and passenger cars under approximate traffic conditions via the Geoapify Isoline API [64]. Mode-specific travel costs

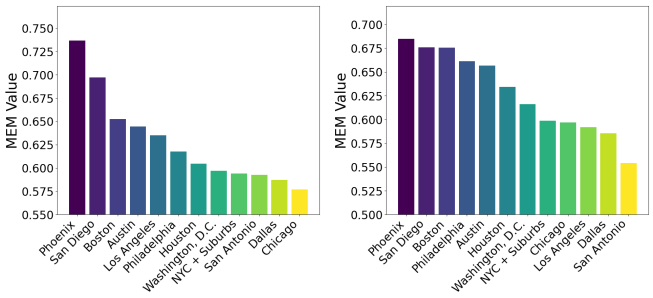

(a) (b)

Fig. 6: MEM values of 12 major cities in the United States: (a) considering all services and (b) only considering essential services

c_m are determined using service fares, vehicle maintenance estimates, or, in the case of walking, assumed as \$0. Price sensitivity κ_i is scaled based on each community's income relative to the city's maximum income, normalizing for cost-of-living differences.

Figure 6a presents MEM results across the 12 cities based on all services in Table II, showing MEM values ranging from 0.577 (Chicago, IL) to 0.737 (Phoenix, AZ). Figure 6b contrasts these with MEM values computed using only essential services (hospitals, pharmacies, schools, and markets), yielding a narrower range from 0.554 (San Antonio, TX) to 0.685 (Phoenix, AZ).

Notably, cities such as Chicago and Philadelphia exhibit improved MEM scores when focusing solely on essential services, reflecting a relatively balanced distribution of critical amenities. Conversely, cities like Los Angeles show decreased essential MEM, suggesting concentrated distributions of vital services. Overall, the comparison reveals that cities with strong reputations for public transit, such as Chicago, may still exhibit significant mobility inequities.

VII. Conclusions

The purpose of this paper has been to make the case for the importance of control, learning, and optimization methods in emerging mobility systems. We have shown how standard optimal control methods provide a natural setting to formulate problems aiming to jointly minimize the three primary objectives in a transportation system: minimize travel times and energy consumption while maximizing passenger comfort, along with guaranteed safety constraints in the operation of CAVs. Since solutions to these problems can become intractable for real-time control, we have also shown how to incorporate Control Barrier Functions (CBFs) to replace complex hard safety constraints by ones that are linear in the control and guarantee the satisfaction of the original constraints as sufficient conditions, thereby introducing a trade-off between safety and performance optimality that can be systematically adjusted. This can be further enhanced through the use of Reinforcement Learning techniques which are the topic of ongoing research [65]. We have also shown how these methods can be extended to mixed traffic where

CAVs must safely interact with HDVs. More broadly, even a partial presence of CAVs can enable new traffic control paradigms. We have discussed how CAVs can act as sensors observing the state of traffic in their vicinity and ultimately also act as actuators to dissipate, for example, traffic congestion. This research direction involves a physics-informed machine learning approach to reconstruct the traffic state needed in designing such controllers. Finally, we have also addressed the societal issues accompanying emerging mobility systems, including new metrics that incorporate accessibility and fairness in a transportation network consisting of both autonomous and human-driven vehicles. In particular, we have introduced a comprehensive Mobility Equity Metric (MEM) based on a node-level Mobility Index (MI) that quantifies accessibility to essential services for travelers from different origin points and captures access disparities across a transportation network.

REFERENCES

[1] M. Mukai, H. Natori, and M. Fujita, "Model predictive control with a mixed integer programming for merging path generation on motor way," in *Proc. IEEE Conference on Control Technology and Applications*, 2017.

[2] M. H. B. M. Nor and T. Namerikawa, "Merging of connected and automated vehicles at roundabout using model predictive control," in *Annual Conference of the Society of Instrument and Control Engineers of Japan*, pp. 272–277, 2018.

[3] W. Xiao, C. G. Cassandras, and C. Belta, *Safe Autonomy with Control Barrier Functions: Theory and Applications*. Springer Nature, 2023.

[4] P. Sardain and G. Bessonnet, "Forces acting on a biped robot. center of pressure-zero moment point," *IEEE Transactions on Systems, Man, and Cybernetics - Part A: Systems and Humans*, vol. 34, no. 5, pp. 630–637, 2004.

[5] W. Xiao and C. G. Cassandras, "Decentralized optimal merging control for connected and automated vehicles with safety constraint guarantees," *Automatica*, vol. 123.109333, 2021.

[6] W. Xiao, C. G. Cassandras, and C. Belta, "Decentralized optimal control in multi-lane merging for connected and automated vehicles," in *Proc. IEEE 23nd Intelligent Transportation Systems Conference*, 2020, pp. 1–6.

[7] W. Xiao and C. G. Cassandras, "Decentralized optimal merging control for connected and automated vehicles with optimal dynamic resequencing," in *Proc. of the American Control Conference*, 2020, pp. 4090–4095.

[8] M. Kamal, M. Mukai, J. Murata, and T. Kawabe, "Model predictive control of vehicles on urban roads for improved fuel economy," *IEEE Transactions on Control Systems Technology*, vol. 21, no. 3, pp. 831–841, 2013.

[9] W. Xiao, C. G. Cassandras, and C. Belta, "Bridging the gap between optimal trajectory planning and safety-critical control with applications to autonomous vehicles," *Automatica*, vol. 129.109592, 2021.

[10] K. Vogel, "A comparison of headway and time to collision as safety indicators," *Accident Analysis & Prevention*, vol. 35, no. 3, pp. 427–433, 2003.

[11] Bryson and Ho, *Applied Optimal Control*. Waltham, MA: Ginn Blaisdell, 1969.

[12] A. D. Ames, J. W. Grizzle, and P. Tabuada, "Control barrier function based quadratic programs with application to adaptive cruise control," in *Proc. of 53rd IEEE Conference on Decision and Control*, 2014, pp. 6271–6278.

[13] W. Xiao, C. G. Cassandras, and C. Belta, "Decentralized merging control in traffic networks with noisy vehicle dynamics: A joint optimal control and barrier function approach," in *Proc. IEEE 22nd Intelligent Transportation Systems Conference*, 2019.

[14] R. Wiedemann, "Simulation des straßenverkehrsflusses," in *Proc. of the Schriftenreihe des tnstituts fir Verkehrswesen der Universitiit Karlsruhe (In German language)*, 1974.

[15] Y. Zhang and C. G. Cassandras, "A decentralized optimal control framework for connected automated vehicles at urban intersections with dynamic resequencing," in *2018 IEEE Conference on Decision and Control (CDC)*. IEEE, 2018, pp. 217–222.

[16] A. Li, A. C. Armijos, and C. G. Cassandras, "Robust optimal lane-changing control for connected autonomous vehicles in mixed traffic," *Automatica*, vol. 174, no. 112169, 2025.

[17] M. Papageorgiou, H. Hadj-Salem, and J. M. Blosseville, "Alinea: A local feedback control law for on-ramp metering," *Transportation Research Record*, vol. 1320, no. 1, pp. 58–67, 1991.

[18] A. Ferrara, S. Sacone, and S. Siri, *Freeway Traffic Modelling and Control*. Springer Nature, 2018.

[19] M. J. Lighthill and G. B. Whitham, "On kinematic waves ii. a theory of traffic flow on long crowded roads," *Proceedings of the Royal Society of London. Series A. Mathematical and Physical Sciences*, vol. 229, no. 1178, pp. 317–345, 1955.

[20] P. I. Richards, "Shock waves on the highway," *Operations Research*, vol. 4, no. 1, pp. 42–51, 1956.

[21] J. P. Lebacque, J. B. Lesort, and F. Giorgi, "Introducing buses into first-order macroscopic traffic flow models," *Transportation Research Record*, vol. 1644, no. 1, pp. 70–79, 1998.

[22] M. L. D. Monache and P. Goatin, "A front tracking method for a strongly coupled pde-ode system with moving density constraints in traffic flow," *Discrete and Continuous Dynamical Systems*, 2014.

[23] M. Čičić, "Modelling and lagrangian control of mixed traffic: platoon coordination, congestion dissipation and state reconstruction," PhD Thesis, KTH Royal Institute of Technology, 2021.

[24] M. Raissi, P. Perdikaris, and G. Karniadakis, "Physics-informed neural networks: A deep learning framework for solving forward and inverse problems involving nonlinear partial differential equations," *Journal of Computational Physics*, vol. 378, pp. 686–707, 2019.

[25] M. Barreau, M. Aguiar, J. Liu, and K. H. Johansson, "Physics-informed learning for identification and state reconstruction of traffic density," in *IEEE Conference on Decision and Control*, 2021.

[26] M. Barreau, J. Liu, and K. H. Johansson, "Learning-based state reconstruction for a scalar hyperbolic pde under noisy lagrangian sensing," in *Learning for Dynamics and Control (L4DC)*, 2021.

[27] M. Behrisch, L. Bieker, J. Erdmann, and D. Krajzewicz, "Sumo – simulation of urban mobility; an overview," German Aerospace Centre, Institute for Transportation Research, Tech. Rep., 2011.

[28] L. Giorgi, "Prise en compte des transports en commune de surface dans la modélisation macroscopique de l'Écoulement du trafic," PhD Thesis, Institut National des Sciences Appliquées de Lyon, 2002.

[29] M. Čičić and K. H. Johansson, "Traffic regulation via individually controlled automated vehicles: a cell transmission model approach," in *International Conference on Intelligent Transportation Systems*, 2018.

[30] R. E. Stern, S. Cui, M. L. D. Monache *et al.*, "Dissipation of stop-and-go waves via control of autonomous vehicles: Field experiments," *Transportation Research Part C*, vol. 89, pp. 205–221, 2018.

[31] M. Čičić and K. H. Johansson, "Front-tracking transition system model for traffic state reconstruction, model learning, and control with application to stop-and-go wave dissipation," *Transportation Research Part B*, vol. 166, 2022.

[32] N. Venkatesh, V.-A. Le, A. Dave, and A. A. Malikopoulos, "Connected and automated vehicles in mixed-traffic: Learning human driver behavior for effective on-ramp merging," in *Proceedings of the 62nd IEEE Conference on Decision and Control (CDC)*. IEEE, 2023, pp. 92–97.

[33] A. Genser, M. A. Makridis, K. Yang, L. Ambühl, M. Menendez, and A. Kouvelas, "Time-to-green predictions for fully-actuated signal control systems with supervised learning," *IEEE Transactions on Intelligent Transportation Systems*, 2024.

[34] A. M. I. Mahbub, V.-A. Le, and A. A. Malikopoulos, "Safety-aware and data-driven predictive control for connected automated vehicles at a mixed traffic signalized intersection," in *10th IFAC International Symposium on Advances in Automotive Control*. IFAC, 2022, pp. 51–56.

[35] A. A. Malikopoulos and L. Zhao, "A closed-form analytical solution for optimal coordination of connected and automated vehicles," in *2019 American Control Conference (ACC)*. IEEE, 2019, pp. 3599–3604.

[36] ——, "Optimal path planning for connected and automated vehicles at urban intersections," in *Proceedings of the 58th IEEE Conference on Decision and Control, 2019*. IEEE, 2019, pp. 1261–1266.

[37] A. A. Malikopoulos, L. E. Beaver, and I. V. Chremos, "Optimal time

trajectory and coordination for connected and automated vehicles," *Automatica*, vol. 125, no. 109469, 2021.

[38] A. M. I. Mahbub and A. A. Malikopoulos, "Conditions to Provable System-Wide Optimal Coordination of Connected and Automated Vehicles," *Automatica*, vol. 131, no. 109751, 2021.

[39] B. Chalaki and A. A. Malikopoulos, "Optimal control of connected and automated vehicles at multiple adjacent intersections," *IEEE Transactions on Control Systems Technology*, vol. 30, no. 3, pp. 972–984, 2022.

[40] ——, "Time-optimal coordination for connected and automated vehicles at adjacent intersections," *IEEE Transactions on Intelligent Transportation Systems*, vol. 23, no. 8, pp. 13 330–13 345, 2021.

[41] B. Chalaki, L. E. Beaver, and A. A. Malikopoulos, "Experimental validation of a real-time optimal controller for coordination of CAVs in a multi-lane roundabout," in *2020 IEEE Intelligent Vehicles Symposium (IV)*. IEEE, 2020, pp. 775–780.

[42] L. Zhao and A. A. Malikopoulos, "Decentralized optimal control of connected and automated vehicles in a corridor," in *2018 21st International Conference on Intelligent Transportation Systems (ITSC)*, Nov 2018, pp. 1252–1257.

[43] A. M. I. Mahbub, A. A. Malikopoulos, and L. Zhao, "Impact of connected and automated vehicles in a corridor," in *Proceedings of 2020 American Control Conference, 2020*. IEEE, 2020, pp. 1185–1190.

[44] A. I. Mahbub, A. A. Malikopoulos, and L. Zhao, "Decentralized optimal coordination of connected and automated vehicles for multiple traffic scenarios," *Automatica*, vol. 117, no. 108958, 2020.

[45] H. Bang and A. A. Malikopoulos, "A hierarchical approach to optimal flow-based routing and coordination of connected and automated vehicles," in *Proceedings of the 62nd IEEE Conference on Decision and Control (CDC)*, 2023, pp. 7100–7105.

[46] H. Bang, B. Chalaki, and A. A. Malikopoulos, "Combined Optimal Routing and Coordination of Connected and Automated Vehicles," *IEEE Control Systems Letters*, vol. 6, pp. 2749–2754, 2022.

[47] I. V. Chremos and A. A. Malikopoulos, "Mobility equity and economic sustainability using game theory," in *2023 American Control Conference (ACC)*, 2023, pp. 1698–1703.

[48] R. Cervero, "Accessible cities and regions: A framework for sustainable transport and urbanism in the 21st century," 2005.

[49] D. O'Sullivan, A. Morrison, and J. Shearer, "Using desktop gis for the investigation of accessibility by public transport: an isochrone approach," *International Journal of Geographical Information Science*, vol. 14, no. 1, pp. 85–104, 2000.

[50] Y. Fan, A. Guthrie, and D. Levinson, "Impact of light-rail implementation on labor market accessibility: A transportation equity perspective," *Journal of Transport and Land use*, vol. 5, no. 3, pp. 28–39, 2012.

[51] A. Golub and K. Martens, "Using principles of justice to assess the modal equity of regional transportation plans," *Journal of Transport Geography*, vol. 41, pp. 10–20, 2014.

[52] G. Tian, Y. D. Wei, and H. Li, "Effects of accessibility and environmental health risk on housing prices: A case of salt lake county, utah," *Applied Geography*, vol. 89, pp. 12–21, 2017.

[53] S. Mavoa, K. Witten, T. McCreanor, and D. O'sullivan, "Gis based destination accessibility via public transit and walking in auckland, new zealand," *Journal of transport geography*, vol. 20, no. 1, pp. 15–22, 2012.

[54] A. El-Geneidy and D. Levinson, "Mapping accessibility over time," *Journal of Maps*, vol. 3, no. 1, pp. 76–87, 2007.

[55] K. Manaugh and A. El-Geneidy, "Who benefits from new transportation infrastructure? using accessibility measures to evaluate social equity in public transport provision," in *Accessibility analysis and transport planning*. Edward Elgar Publishing, 2012, pp. 211–227.

[56] J. Grengs, J. Levine, Q. Shen, and Q. Shen, "Intermetropolitan comparison of transportation accessibility: sorting out mobility and proximity in san francisco and washington, dc," *Journal of Planning Education and Research*, vol. 29, no. 4, pp. 427–443, 2010.

[57] A. El-Geneidy, D. Levinson, E. Diab, G. Boisjoly, D. Verbich, and C. Loong, "The cost of equity: Assessing transit accessibility and social disparity using total travel cost," *Transportation Research Part A: Policy and Practice*, vol. 91, pp. 302–316, 2016.

[58] H. Bang, A. Dave, and A. A. Malikopoulos, "Routing in Mixed Transportation Systems for Mobility Equity," *Proceedings of the 2024 American Control Conference*, pp. 1486–1491, 2024.

[59] H. Bang, A. Dave, F. Tzortzoglou, and A. A. Malikopoulos, "A mobility equity metric for multi-modal intelligent transportation systems," 2024, pp. 114–119.

[60] H. Bang, A. Dave, F. Tzortzoglou, S. Wang, and A. A. Malikopoulos, "On mobility equity and the promise of emerging transportation systems," *IEEE Transactions on Intelligent Transportation Systems*, 2024 (in review).

[61] Y. Xi, E. J. Miller, and S. Saxe, "Exploring the impact of different cut-off times on isochrone measurements of accessibility," *Transportation Research Record*, vol. 2672, no. 49, pp. 113–124, 2018.

[62] U. S. C. Bureau, "Census data api: Variables in /data/2010/acs/acs5/spt/variables," 2010, accessed: 2023-04-01. [Online]. Available: https://api.census.gov/data/2010/acs/acs5/spt/variables.html

[63] TOMTOM, "Pointes of interest search," 2023, accessed: 2023-04-01. [Online]. Available: https://developer.tomtom.com/search-api/documentation/search-service/points-of-interest-search

[64] Geoapify, "Isoline api playground," 2024, accessed: 2023-04-01. [Online]. Available: https://apidocs.geoapify.com/playground/isoline/

[65] E. Sabouni, H. Ahmad, V. Giammarino, C. Cassandras, I. Paschalidis, and W. Li, "Reinforcement learning-based receding horizon control using adaptive control barrier functions for safety-critical systems," in *63rd IEEE Conference on Decision and Control*. IEEE, 2024, pp. 401–406.